Atmos. Chem. Phys. Discuss., 2, 1655–1697, 2002
www.atmos-chem-phys.org/acpd/2/1655/
© European Geosciences Union 2002

Atmospheric Chemistry and Physics Discussions

The Hohenpeissenberg aerosol formation experiment (HAFEX): a long-term study including size-resolved aerosol, H_2SO_4, OH, and monoterpenes measurements

W. Birmili[1], H. Berresheim[2], C. Plass-Dülmer[2], T. Elste[2], S. Gilge[2], A. Wiedensohler[3], and U. Uhrner[3]

[1]University of Birmingham, Division of Environmental Health and Risk Management, Birmingham, B15 2TT, UK
[2]German Weather Service, Meteorological Observatory Hohenpeissenberg (MOHp), Albin-Schwaiger-Weg 10, 83282 Hohenpeissenberg, Germany
[3]Institute for Tropospheric Research, Permoserstrasse 15, 04303 Leipzig, Germany

Received: 11 September 2002 – Accepted: 6 October 2002 – Published: 28 October 2002

Correspondence to: W. Birmili (w.birmili@bham.ac.uk)

© EGU 2002

Abstract

Ambient aerosol size distributions (> 3 nm) and OH, H_2SO_4, and terpene concentrations were measured from April 1998 to August 2000 at a rural continental site in southern Germany. New particle formation (NPF) events were detected on 18% of all days, typically during midday hours under sunny and dry conditions. Surprisingly, most NPF events occurred during spring and winter, whereas the concentrations of aerosol precursors (H_2SO_4, monoterpenes) clearly peaked in summer. The number of newly formed particles correlated significantly with solar irradiance and ambient levels of H_2SO_4 and anti-correlated, especially in the cold season, with relative humidity and the condensational sink provided by pre-existing particles. The particle formation rates were experimentally estimated to be on order of $1\,cm^{-3}\ s^{-1}$. Binary homogeneous H_2SO_4-H_2O nucleation rates calculated from measured H_2SO_4 were substantially lower than this, even if assuming particle formation under the thermodynamic conditions on top of the boundary layer. The nucleation mode particle growth rates derived from the evolution of the size distribution were $2.6\,nm\,h^{-1}$ on average, with a fraction of $0.7\,nm\,h^{-1}$ attributed to the co-condensation of $H_2SO_4/H_2O/NH_3$. Turn-over rate calculations of measured monoterpenes and aromatic hydrocarbons suggest that especially the oxidation products of monoterpenes may contribute to the observed particle growth, although no indications were found that the reaction products of organic compounds would generally control the occurrence of NPF events.

1. Introduction

Atmospheric particulates, contributing to light scattering, cloud formation, and heterogeneous chemical reactions, are a key factor in the global climate system (Haywood and Boucher, 2000; Ravishankara, 1997). An important contribution to atmospheric particle number concentration is the homogeneous nucleation of supersaturated vapours. Its feedback on global climate, however, is still uncertain, although

ACPD

2, 1655–1697, 2002

© EGU 2002

potentially large and opposite to the warming effect of greenhouse gases (Houghton et al., 2001). The formation of new particles by gas-to-particle conversion has been extensively studied in the remote marine and Arctic environment (Covert et al., 1992; Raes, 1995; Wiedensohler et al., 1996; Weber et al., 1999), in the free troposphere (Clarke, 1993), and in continental regions (Weber et al., 1997). In coastal regions a source related to biogenic iodine emissions has been identified (O'Dowd et al., 2002a). In the well-mixed continental boundary layer particle formation is typically observed to be followed by subsequent particle growth occurring in relatively homogeneous air masses extending over large areas (Mäkelä et al., 1997; Hõrrak et al., 1998; Birmili and Wiedensohler, 2000; Kulmala et al., 2001). However, our present understanding of the mechanism of new particle formation in the atmosphere is still uncertain. Several particle nucleation and growth mechanisms have recently been proposed: (1) involvement of ammonia in the nucleation process, in addition to H_2SO_4 and H_2O, (ternary nucleation; Coffman and Hegg, 1995); (2) ubiquitous existence of thermodynamically stable clusters, possibly formed from ternary nucleation (Kulmala et al., 2000), with particle growth being dominated by oxidation products of biogenic organic vapours such as terpenes or amines (O'Dowd et al., 2002b); (3) ion-induced or ion-mediated nucleation and growth (Yu and Turco, 2000); (4) enhancement of nucleation by small-scale turbulent atmospheric mixing (Easter and Peters, 1994; Nilsson and Kulmala, 1998). However, to this date no physical model has been developed and validated for a wide range of NPF events. The acquisition of new knowledge is mainly deterred due to the scarcity of long-term studies, and present instrumental shortcomings such as the inability to count freshly nucleated particles (< 3 nm), and to determine their chemical composition. Moreover, sensitive and high-time-resolution techniques have been missing to measure precursor gases (e.g. H_2SO_4, NH_3, organics) at accuracies required for atmospheric studies.

In the Hohenpeissenberg Aerosol Formation Experiment (HAFEX), recently developed techniques were simultaneously applied for the first time to measure atmospheric concentrations of H_2SO_4, OH, terpenes and aromatic hydrocarbons and to investigate

ACPD
2, 1655–1697, 2002

© EGU 2002

the potentially important roles of these compounds in the formation and growth of new particles. The results are unique in that they are based on a combination of these measurements over the course of 2.5 years.

2. Experimental

2.1. Measurement site and program overview

The HAFEX measurement program was conducted at the Meteorological Observatory Hohenpeissenberg (MOHP; 47° 48′ N, 11° 07′ E), a Global Atmosphere Watch (GAW) site and mountain station operated by the German Weather Service (DWD). The observatory is located on top of the Hohenpeissenberg mountain (980 m above sea level) and about 300 m above the surrounding countryside. The nearest major city, Munich, is distant at ca. 60 km. MOHp is surrounded mainly by forests and agricultural pastures with coniferous trees and beeches growing on the slopes of the Hohenpeissenberg mountain in most directions. Air was sampled through inlets at 10 m above ground level, roughly corresponding to the height of the canopy. Particle size distributions, sulphuric acid and OH concentrations were measured continuously between 1 April 1998, and 3 August 2000, with occasional interruptions due to maintenance. Terpenes and hydrocarbons were measured on an hourly basis during specific periods and once a day whenever possible. During a 6-week period in April and May 1999, the particle size distribution was additionally measured at a second field station at the foot of the Hohenpeissenberg mountain. The horizontal and vertical distances between the two sites were approximately 3 km and 300 m, respectively. The long-term study was also supported by routine meteorological and atmospheric chemical measurements at MOHp, as part of the GAW program (WMO2001), and regular radiosonde ascent data from DWD's station at Munich.

ACPD
2, 1655–1697, 2002

© EGU 2002

2.2. Particle number size distributions

Particle number size distributions (3–800 nm) were continuously recorded over 10–15 min intervals with a Twin Differential Mobility Particle Sizer (TDMPS) (Birmili et al., 1999). The TDMPS system is based on two Vienna-type differential mobility analysers (DMAs) (Winklmayr et al., 1991). Monodisperse particles were counted downstream of the DMAs with condensation particle counters (CPC; models UCPC 3025A and CPC 3010, respectively; TSI Inc., St Paul, MN, USA). Ambient air was sampled at 16.7 l min^{-1} through a PM_{10} Anderson impactor inlet and stainless steel tubing. Inversion of mobility into size distributions accounted for the bipolar charge distribution, and empirically determined transfer functions of the DMAs and CPCs. Particles were additionally counted using two stand-alone CPCs having different lower particle size detection limits (TSI models 3025A and 3010, respectively). In the TDMPS, particles were dried and classified at relative humidities below 10%. To reconstruct a particle size distribution at ambient relative humidity (RH), a hygroscopic growth model was applied relating the "wet" and "dry" particle sizes at given RH:

$$D_p(\mathrm{RH}) = D_{p,0} \cdot (1.0 + 5.0 \cdot (1 - \mathrm{RH})^{-1}) \quad (1)$$

The coefficients of this equation were determined from measurements of particle hygroscopicity with a Tandem Differential Mobility Analyser at Hohenpeissenberg in 1997 and 1998 (Karg et al., 1999). Equation (1) refers to the "more hygroscopic" fraction of aerosol particles (the dominating number fraction at Hohenpeissenberg), and was derived from data based on 50 nm particle size. Equation (1) deviates from that most frequently found in literature (Swietlicki et al., 1999), but we chose the present form because it provided a superior fit to the experimental data.

2.3. H_2SO_4 and OH

Gas phase H_2SO_4 and OH concentrations were measured by atmospheric pressure chemical ionisation mass spectrometry (AP/CIMS) (Berresheim et al., 2000). Briefly,

ACPD
2, 1655–1697, 2002

© EGU 2002

OH radicals were titrated by excess $^{34}SO_2$ to form $H_2{}^{34}SO_4$. Both $H_2{}^{34}SO_4$ and ambient H_2SO_4 ($\approx$ 96% consisting of $H_2{}^{32}SO_4$) were chemically converted to the corresponding HSO_4^- ions by reaction with NO_3^- ions. A measurement cycle typically consisted of 20 min of continuous H_2SO_4 measurements (30 s time resolution), followed by 5–10 min of OH measurements. For 5 min signal integration, conservative estimates of the detection limits of H_2SO_4 and OH were $3 \cdot 10^4$ and $5 \cdot 10^5$ molec. cm^{-3}. The overall accuracy (2σ) of the method was estimated to be 39% and 54%, respectively.

2.4. Monoterpenes and aromatic hydrocarbons

Monoterpenes and aromatic hydrocarbon (C_6-C_{10}) concentrations in ambient air were measured on-line by gas chromatography ion-trap mass spectrometry (GC-MS, Varian, Palo Alto, CA). Details of the system are to be presented in a future paper. Briefly, air samples were taken from a permanently flushed glass sample line (length: 10 m, ø 4 cm) and passed through a sodium thiosulfate ($Na_2S_2O_3$) impregnated glass fibre filter to remove ozone. Hydrocarbons were adsorbed in a Carbopack B (Supelco) trap at 40°C, desorbed at 230°C, and cryo-focussed in a silco-steel capillary (ø 0.28 mm) at 77 K. After thermal flash-desorption at 180°C hydrocarbons were separated on a capillary column (BPX-5, length: 50 m, ø 0.22 mm, 1 μm film) and detected by MS. The detection limits were below 2 pptv for air samples of 1.5 liters. The measurement uncertainties were < 30% for aromatics, and 30–50% for monoterpenes. Daily samples were taken at approximately 13:00 h, and more often during intensive measurement periods. The above experimental set-up was used from the year 2000. During the years 1998–99, different adsorbent material (Carbopack C) and desorption procedures were used which caused additional losses and interconversion between different terpenes. Therefore, all aromatic hydrocarbon data shown in this paper refer to the entire HAFEX period, but terpene data only to the year 2000.

ACPD
2, 1655–1697, 2002

© EGU 2002

3. New particle formation events: observations

3.1. Three case studies

Figure 1 shows three examples of new particle formation (NPF) including the time evolution of the particle size distribution, ultrafine particle (UFP) concentrations (size range 3–11 nm), total particle, H_2SO_4 and OH concentrations. The examples illustrate the dynamic range of NPF "events" that occurred during the 2.5 year measurement period. Indeed, we observed a continuum of observations, ranging from pronounced NPF events (Fig. 1, 15 May 1998) to such phenomena that are on the limit of being classified as "event" (Fig. 1, 7 April 2000). The concentrations of ultrafine particles (UFP) were generally low at night-time. In case of a particle formation event, high UFP concentrations occurred predominantly around noon (median: 12:53 h; quartile range: 11:53 h–13:45 h). UFP concentrations peaked around 30 000 cm^{-3} (15 May 1998), 6000 cm^{-3} (25 March 1999), and 2000 cm^{-3} (7 April 2000). H_2SO_4 and OH showed pronounced diel cycles as well, with maximum concentrations between 1 and $2 \cdot 10^7$ cm^{-3} around noon in the cases shown in Fig. 1. During NPF events, the diameters of maximum particle concentration often shifted from initially 3–8 nm to larger diameters over several hours, occasionally approaching 20 nm or more on the same day. This shift was clearly evident on 15 May 1998, although less pronounced on 25 March 1999 and 7 April 2000. Due to the regularity of this observation, this diameter shift is assumed to be the result of condensational growth of freshly nucleated particles over a large area. A third feature of NPF events was that after passing through the concentration maximum the concentration of UFPs decreased again, at an average characteristic time (decrease to $1/e$) of 2.4 h (full range: 0.4–6.4 h). A major process responsible for this removal of UFPs has been found to be coagulation with larger particles (e.g. Birmili et al., 2000; Kerminen et al., 2001).

ACPD
2, 1655–1697, 2002

© EGU 2002

3.2. Particle formation events: spatial extension

Knowledge about the spatial scale of NPF events as a meteorological phenomenon can be helpful in the search for the possible particle sources. Here, we estimated the horizontal extension of air parcels in which NPF events occurred by multiplying the time during which a clear trace of the nucleation mode diameter could be seen, and the locally measured wind speed. This yielded an average extension of 87 km (minimum: 6 km, maximum: 339 km) suggesting that NPF events are a mesoscale phenomenon. A vertical distribution of NPF events, in contrast, is more difficult to assess unless airborne measurements are performed. To approach this problem, however, we measured particle size distributions concurrently at two different altitudes: at MOHp (980 m) and, additionally, at a site at the foot of the Hohenpeissenberg mountain (680 m). Figure 2 shows the evolution of a NPF event measured simultaneously at both sites, and illustrates that the particle size spectra and total concentrations evolved in very similar fashion at both altitudes. Using the time series of total particle counters (UCPC 3025) deployed at both altitudes, a time lag of less than 5 min was determined between the curves of N_{tot} at the both sites. This example demonstrates the similarity in the behaviour of UFPs at the different sites, and suggests a very homogeneous distribution of newly formed particles in the lower section (300 m) of the boundary layer.

3.3. Shape of the particle size distribution

The shape of the particle size distribution during NPF events can be seen in Fig. 3: The maxima in the size distributions are always between 5 and 10 nm with decreasing concentrations towards smaller sizes, which is not an effect of the logarithmic size scale. While such "closed" distributions during or after atmospheric particle bursts have been observed by other research groups using very similar TDMPS systems (e.g. Coe et al., 2000; Kulmala et al., 2001), measurements in an urban atmosphere in Atlanta have yielded particle size distributions that monotonically increase towards smaller particles (McMurry et al., 2000), which is the shape that would theoretically be expected assum-

© EGU 2002

ing a continuous supply of nucleating particles. To scrutinise the possible impact of measurement artefacts in UFP range on our measurements we deployed, during much of the duration of HAFEX, a combination of two condensation particle counters (CPCs) using different lower detection limits (∼3 and 11 nm, respectively). This allowed to determine particle concentrations independently from the TDMPS. Sample data for an event on 26 December 1998 is shown in Fig. 4, where it can be seen that the different particle concentration profiles derived from both systems, including UFP concentrations, agreed within 10%. The measurement uncertainty of the TDMPS technique includes at least the following uncertainties: CPC counting efficiency, ∼ 10% (after individual calibration of an instrument); DMA transfer function, ∼ 20% (e.g. Reischl et al., 1997; Birmili et al., 1997); bipolar charge distribution, ∼ 20% (Wiedensohler, 1988). These estimates refer to the accuracy of a concentration measurement at the size 5 nm. Taking into account that CPC technology is more simple and less prone to possible nano-particle losses than the electrical classifier, we found no evidence to suggest that the measured "closed" nano-particle size distributions during HAFEX would be incorrect. Obtaining the correct nano-particle size distribution shape is essential with regard to the conclusions where the particles may actually have nucleated.

4. New particle formation events: classification and correlations with atmospheric parameters

4.1. NPF event classification

For a systematic evaluation of the 2.5-year data set, we defined the occurrence of new particle formation "events" based on the time histories of ultrafine (3–11 nm) and total particle (≥ 3 nm) concentrations ($N_{[3;11]}$ and N_{tot} hereafter). $N_{[3;11]}$ and N_{tot} were usually determined by numerical integration from the measured particle size distributions. Figure 5 illustrates three major characteristics of a diurnal cycle of $N_{[3;11]}$: (1) a rapid increase from low levels to near the daily maximum, (2) a plateau range where variations

ACPD
2, 1655–1697, 2002

© EGU 2002

in concentration remain limited, and (3) a subsequent decline in $N_{[3;11]}$. By numerical curve fit, these characteristics were conveyed into four parameters that serve as a basis to classify all observed diurnal profiles into events and non-events: (a) a "plateau" (≈ daily maximum) concentration, (b) a characteristic time for the curve to rise, (c) a characteristic time for the curve to decline, and (d) the fraction of UFPs during the event, i.e. the quotient $N_{[3;11]}/N_{tot}$. See Fig. 5 for an illustration of the parameters (a)–(c). To be classified as a NPF event, the parameters (a)–(d) of an individual diurnal cycle had to satisfy the specific range criteria, given in Table 1. Next, the plateau (maximum) concentration (a) was used to categorise all NPF events into 3 classes (I, II, III) representing different UFP maximum concentrations: Event class I (> 7000 cm^{-3}), class II (2500–7000 cm^{-3}), and class III (1000–2500 cm^{-3}). The application of the above described schemes yielded 117 NPF events out of a total of 651 days, which means that particle formation events occurred on approximately 18% of all days. 19 events were ranked class I, 49 class II, and 49 class III. These numbers are shown in Fig. 6, keyed after the different seasons. NPF events occurred most frequently in winter (25% event probability) and spring (21%) but interestingly, least frequently in summer (12%). Particularly, no class I event was observed in summer, which was surprising with regard to the expectation that the photochemically produced vapour reservoir would be most intense in that season. Finding a high seasonal event frequency in spring is shared by other statistical descriptions of NPF events over continental areas (Mäkelä et al., 2000; Birmili and Wiedensohler, 2000; Hõrrak et al., 2000), but a frequent occurrence of wintertime events such as at Hohenpeissenberg has not been reported yet.

4.2. Variations of H_2SO_4, OH, meteorological parameters, and the condensational sink

Median diurnal cycles of H_2SO_4 and OH concentrations and meteorological parameters were calculated (see Fig. 7). Because of the seasonal influence of boundary layer convection, the data were divided into two blocks comprising the "warm" season (March–October) and the "cold" season (November–February), respectively. In

ACPD
2, 1655–1697, 2002

© EGU 2002

the warm season, H_2SO_4 concentrations correlate with the intensity of NPF events (Fig. 7). The highest event class (I) shows daily maximum H_2SO_4 concentrations above 10^7 molec. cm^{-3}, whereas the event classes II and III were associated with peak concentration of $5 \cdot 10^6$ and $3 \cdot 10^6$ cm^{-3}, respectively. Event class III concentrations were similar to non-event concentrations. The cold season was different in that H_2SO_4 typically peaked between 6 and $8 \cdot 10^6$ cm^{-3} for all event classes (I-III) whereas on non-event days, only $\sim 2 \cdot 10^6$ cm^{-3} were measured. Although the hydroxyl radical (OH) concentration showed a pronounced seasonal behaviour – with daily maxima typically around $\sim 4 \cdot 10^6$ cm^{-3} in the warm season, but only $2 \cdot 10^6$ cm^{-3} in the cold season – it shows less distinction between event and non-event days. An exception is event class I in the warm season when OH concentrations reached up to $7 - 8 \cdot 10^6$ cm^{-3} between 09:00 h and 12:00 h. These days also tended to show increased mid-day ozone concentrations (60 ppbV, ca. 20 ppbV more than on non-event days), pointing out the relevance of photochemical processes to provide gaseous aerosol precursors on class I event days. In order to distinguish between cloudy days and clear skies, the solar irradiance measurement was normalised by a monthly cloudless reference profile. Accordingly, a radiation value of 1 refers to a clear sky. Figure 7 shows that the particle formation intensity correlated with solar irradiance, and anti-correlated with relative humidity (RH), especially in the cold season. While the correlation with solar irradiance is plain to understand in terms of photochemical processes generating aerosol precursors, the significant anti-correlation with RH is not. From nucleation theory, particle formation would be rather eased by *high* relative humidities. Low relative humidities are often the result of high temperatures caused by intense solar radiation, and may therefore largely be considered a lateral effect of solar radiation.

A further factor related to the formation of new particles is the pre-existing particle surface area, which is also RH dependent. The pre-existing particle surface area competes with the particle nucleation process for condensable vapours. The measure for this competition is the "condensational sink flux" (CS_{wet}) of condensable vapours onto the pre-existing particles population. CS_{wet} was calculated with the measured parti-

ACPD
2, 1655–1697, 2002

© EGU 2002

cle size distribution adjusted to ambient relative humidity using the hygroscopic growth model from Sect. 2.2 above. The mass transfer equations included the Dahneke Kernel (Seinfeld and Pandis, 1998), H_2SO_4 molecular diffusivity at ambient temperature, an accommodation coefficient of unity. The diurnal cycles of CS_{wet} as a function of the NPF event class are displayed in the bottom graph of Fig. 7: In the warm season, CS_{wet} was by typically 20% lower on NPF event days compared to non event-days, which is weak evidence for an inhibitive effect of a pre-existing particle surface area on the particle formation process. The effect is even more significant for NPF events in the cold season where CS_{wet} is lower by up to 80% compared to non event-days. In the cold season it appears that a combination of sufficient solar radiation and a low pre-existing CS_{wet} are responsible for the developement of the NPF events. Based on back-trajectory analysis, the class I events in the cold season were, in most cases, associated with the advection of southerly, warm air masses that subsidised in the vicinity of the Alpine mountain range. A consideration of anthropogenic tracers (mixing ratios of CO, NO, not shown) suggests that the low CS_{wet} on class I and II events before 1000 h (cf. Fig. 7) are the result of the MOHp mountain site residing in an air layer above the surface inversion, which shows a lower pre-existing particle population. These observations were the strongest association between NPF and meteorological events we identified in the HAFEX data set.

4.3. Statistical significance of the relation between NPF events, H_2SO_4 and solar irradiance

The relationship between the particle formation intensity and H_2SO_4 was examined with statistical tests. To ease statistical treatment, daily maximum values of H_2SO_4 and solar irradiance were determined by fitting Gaussian curves to each daily cycle. These daily maximum values were then compared to the observed UFP maximum concentration (i.e. the plateau values of $N_{[3;11]}$), as can be seen in Fig. 8 for H_2SO_4. The statistical confidence that event days are linked with increased H_2SO_4 was 99.99% for class I events, 99% for class II events but less than 90% and, thus, not significantly for

© EGU 2002

class III events (see Table 2). Before testing the same hypothesis on solar irradiance, the diurnal cycles of solar irradiance were normalised by a cloudless radiation profile of the respective month (cf. Fig. 7) in order to better distinguish between cloudy and clear days over the entire annual cycle. While the solar irradiance intensity was less significantly correlated to the observed UFP maximum concentrations without normalisation, it proved to be a superior indicator of particle formation for all event classes I–III including this normalisation (see Table 2). Despite NPF events being significantly associated with increased H_2SO_4 and solar irradiance, the wide scatter in data such as H_2SO_4 for the class I (cf. Fig. 8) clearly demonstrates that there is no lower threshold criterion in H_2SO_4 that would trigger a NPF event. Indeed the lowest H_2SO_4 peak concentration observed during a class I event (27 January 2000) was as low as $2.8 \cdot 10^6\,\mathrm{cm}^{-3}$. A similar scatter of data involving similar conclusions was observed in case of solar irradiance.

4.4. The concept of vapour availability

Based on the findings of the previous sections we extend the analysis to condensable species of photochemical origin in general (with vapour pressures similar to H_2SO_4), and introduce the quantity "vapour availability" X. A similar approach was proposed by Clement et al. (2001) to study the onset and cut-off criteria of NPF events at a Finnish boreal forest site. The vapour availablity X is defined as

$$X = \text{solar flux} \,/\, \mathrm{CS}_{\mathrm{wet}}, \qquad (2)$$

$\mathrm{CS}_{\mathrm{wet}}$ being the condensational sink flux of condensable vapours described above. Equation (2) is the variant of a steady-state mass balance equation, balancing a source and a sink term of a photochemically produced condensable vapour, resolved after X, the latter therefore representing an equilibrium vapour concentration. Figure 9 compares the daily peak values (determined by Gaussian fits as in the preceding section) of the vapour availability X_{norm} and the monthly normalised solar irradiance (cf. Fig. 7). By requiring $X_{\mathrm{norm}} > 280\,\mathrm{s}$ and $\mathrm{Global}_{\mathrm{norm}} > 0.6$ (see Fig. 9), a parameter space could

ACPD
2, 1655–1697, 2002

© EGU 2002

be defined that encompasses 90% of all class I-II events, while only allowing for 6% of the non-events. This relatively powerful separation resulted solely for the cold season data. In the warm season no such parameter space could be established, suggesting that in that the evolution of NPF events depends less critically on the shown combination of high solar irradiance and low pre-existing particle population.

5. Estimates of the particle formation rate

5.1. Experimental results

Assuming spatial atmospheric homogeneity, particle formation rates were experimentally determined by dividing an observed increase in particle number concentration by the elapsed time: $J_{exp} = N_{uf}/\Delta t$. In Fig. 10, results of J_{exp} are compared for different UFP size ranges, with the upper size sut-offs 3.6, 4.9, 6.6, 8.7, 11.6, 15.5, and 20.6 nm. The lower size cut-off defining UFP range was always 2.8 nm, i.e. the lower detection limit of the TDMPS. The results are shown in Fig. 10, suggesting that the experimental particle formation rate J_{exp} determined from the HAFEX measurements was mostly in the range 0.1–3 $cm^{-3}\,s^{-1}$. J_{exp} does not appear to depend on the choice of the size interval, so we used the rate based on the interval 3–11 nm, introduced earlier in Sect. 4.1, in the following.

5.2. Binary H_2SO_4/H_2O nucleation rate

The experimental particle formation rate was compared to an in-situ binary homogeneous nucleation rate of H_2SO_4 and H_2O. More complex nucleation theories exist involving ammonia (Korhonen et al., 1999), or would be desirable (e.g. for organic vapours) but their applicability is currently limited. Here we test the validity of the binary H_2SO_4/H_2O nucleation rate, which can readily be calculated for in-situ conditions from the H_2SO_4, RH and temperature measurements. The binary rate was computed

© EGU 2002

using a parametrisation of the classical model (Kulmala et al., 1998). The nucleation rates were calculated for 15 min averages of H_2SO_4 concentrations including data from 30 min before the beginning of a formation event until the time the plateau of $N_{[3;11]}$ was reached (cf. Fig. 5). Both the theoretical H_2SO_4/H_2O nucleation rate and the production rate derived from the measurements are compared in Fig. 11. While the experimental formation rates ranged between 0.013 and 8.8 $cm^{-3}\,s^{-1}$, the binary rates were lower by many orders of magnitude, ranging between $8.6 \cdot 10^{-32}$ and $4.5 \cdot 10^{-6}\,cm^{-3}\,s^{-1}$. As expected, the predicted binary rates are higher in the cold season, when the temperatures are lower and the relative humidities higher. On a few events in the cold season, the two rate measurements were close within a few orders of magnitude. Under such conditions binary homogeneous nucleation may provide a qualitative explanation of the observations.

5.3. Particle formation near the top of the boundary layer?

With respect to the high rate discrepancies discussed in the previous section, we tested the hypothesis of H_2SO_4/H_2O nucleating near the top of the boundary layer (TBL) where temperatures may be considerably lower and relative humidities higher. Binary nucleation rates were calculated as above, now using the thermodynamic conditions of the TBL region, estimated from the 13:00 h radioascent at the DWD station Munich (70 km north-east to Hohenpeissenberg) using the simple parcel method and an excess temperature of 0.5 K (Holzworth, 1964). H_2SO_4 was assumed to be well mixed across the boundary layer depth. The analysis was restricted to data from the warm season when the boundary layer depth could be considered to be defined by thermal convection. Figure 12 shows the results: In most cases, the H_2SO_4/H_2O nucleation rate J is predicted to be significantly higher in the TBL region compared to ground level. This holds especially for the medium range of ground level rates in the range $10^{-28} < J < 10^{-13}\,cm^{-3}\,s^{-1}$, where an enhancement by at most 14 orders of magnitude was found. None of the calculated rates, however, exceeds $10^{-4}\,cm^{-3}\,s^{-1}$, and we therefore conclude that the rate discrepancy cannot be explained by this thermody-

ACPD
2, 1655–1697, 2002

© EGU 2002

namic effect alone. Further, the predicted binary rates were not obviously influenced by the class of a NPF event (see Fig. 11). Given the significant discrimination between events and non-events in terms of H_2SO_4 (Fig. 7), the failure to explain such a simple trend indicates a fundamental restriction in the picture of H_2SO_4/H_2O-caused particle formation.

5.4. Ternary nucleation: a discussion

A ternary nucleation process ($H_2SO_4/H_2O/NH_3$) has been predicted to require around 2 orders of magnitude less H_2SO_4 than the binary process (Korhonen et al., 1999), and would qualitatively close the rate discrepancy found between the binary and experimental particle formation rate. Annual median values of ammonia around 6 ppbV have been reported from a rural site in East Germany (Spindler et al., 2001), an area with ammonia sources on a comparable level to Hohenpeissenberg . A concentration of 6 ppbV corresponds to roughly $2 \cdot 10^{11}$ cm^{-3} NH_3 which is 10^4 times more than the H_2SO_4 maximum concentration observed at Hohenpeissenberg. Supposing ammonia to be available in excess within the mixed layer, high nucleation rates would, however, be predicted from measured H_2SO_4 on most of the days at Hohenpeissenberg (including non-event days), which is not in agreement with the observations. Kulmala et al. (2000) suggested a solution to this problem in that the scavenging intensity of nucleation mode particles by pre-existing particles could control whether thermodynamically stable clusters would ever grow into detectable sizes $\sim$ 3 nm or not. From a simplistic consideration of the pre-existing sink for nucleation mode particles to coagulate, however, no uniform picture evolved from the HAFEX data. To provide more insight into the processes controlling NPF events, a more detailed modelling of the particle growth process may be required in future work.

© EGU 2002

6. Estimates of the particle growth rate

6.1. Results derived from experimental observations

During HAFEX, a growth of the nucleation mode particles was frequently observed over the course of several hours after the initial appearance of the mode (see Fig. 13). To quantify this effect, the particle size distributions were individually parametrised by multiple lognormal functions using a least squares algorithm, thus yielding a time series of the nucleation, Aitken, and accumulation mode diameter for each event. As illustrated in the example in Fig. 13, the diameter of the nucleation mode growth often increased in a fashion close to linear with time. The linear fit in the case of Fig. 13 yielded a growth rate of 2.1 nm h^{-1}. From the theory of mass transfer in the continuum regime, a linear growth is consistent with a constant concentration of condensable vapours (Friedlander, 2000). Experimentally, the time of linear particle growth mostly coincided with the time when H_2SO_4 was near its daily peak. Occasionally, however, the growth was observed to continue beyond that period (Fig. 13, after 16:00 h), a phenomenon that is unlikely to be explained by the condensation of short-lived photochemically produced vapours that show a symmetric diurnal cycle around noon. Although linear growth behaviour was occasionally observed for particles as large as 20 nm, the linear fit concentrated on the data in the lowest particle size range, 3–10 nm, i.e. as close as possible to the size of the critical particle embryos. Not all NPF events could be analysed by the method described above; particularly class III were excluded from the analysis because of low particle concentrations and the lack of a clear trace of the nucleation mode diameter with time. Figure 14a displays the annual distribution of the growth rates determined for 71 events evaluated. The entire range of growth rates spanned 0–9 nm h^{-1} with an overall mean of 2.61±0.20 nm h^{-1}. Importantly, the growth rates were limited during the months October to February ($\leq$ 3 nm h^{-1}), leading to a seasonal cycle with increased growth rates in summer (Fig. 14a). This observation is at first sight consistent with the stronger presence of vapour phase precursors as a result of enhanced photochemical activity but also increased organic precursor emis-

ACPD
2, 1655–1697, 2002

© EGU 2002

sions from the biosphere. On the other hand, this result is in contrast to the reduced frequency and intensity of new particle formation in summer, shown earlier in Fig. 6.

6.2. Particle growth by $H_2SO_4/H_2O/NH_3$ condensation

Since direct measurements of sulphuric acid were available, it was possible to estimate its contribution to the particle growth rate. Here, measured H_2SO_4 was assumed to co-condense with H_2O, being neutralised by NH_3 in a 2:1 molar ratio (Birmili et al., 2000). The limiting factor in the growth rate is assumed to be the diffusion of molecular H_2SO_4 onto the pre-existing particles at their ambient size. Ammonia is supposed to be sufficiently available as explained above. The calculated H_2SO_4/NH_3 rate was finally averaged over the time interval corresponding to the linear observed growth of the nucleation mode. Figure 15 shows the two growth rates for the 49 events when H_2SO_4 data were available. Overall, the two rates show little agreement, which indicates that the atmospheric particle growth rate measured during HAFEX must contain significant contributions other than H_2SO_4/NH_3. The four points on the left of the unity curve are attributed to shortcomings in the nucleation mode diameter fit method or to limitations of the one-point observation. The overwhelming majority of data points lie to the right of the unity curve, therefore allowing to describe the growth of the nucleation mode as a composition of one term describing H_2SO_4/NH_3 condensation (0.7 nm h^{-1} on average), and another term, a "missing growth rate", representing the difference between the two growth rates (1.9 nm h^{-1} on average). The cycle of the missing growth rate is shown in Fig. 14b. Most missing growth rates were between 0 and 2 nm h^{-1}, which is indicative of an additional source of condensable vapours throughout the year. 8 data points occurred above 3.0 nm h^{-1}, notably all between April and September. These might point to an independent source of condensable vapours, which would be predominantly active in the warm season.

ACPD
2, 1655–1697, 2002

© EGU 2002

6.3. The potential contribution of monoterpenes and aromatics

Figure 16a shows the seasonal cycles of monoterpene and aromatic hydrocarbon concentrations during HAFEX. Aromatic hydrocarbons were most abundant in winter and the least in summer. Since their seasonal cycle is inverse to that of OH (cf. Fig. 7), the calculated turn-over rates due to reactions with OH did not show a pronounced seasonal cycle (see Fig. 16b). Terpenes, in contrast, showed the highest mixing ratios in summer (Fig. 16a) due to their temperature-dependent biogenic source intensity (Guenther et al., 1993). Since OH and ozone concentrations also peak in summer, the highest turn-over rates were determined for the summer months, for instance $6.0 \pm 5.1 \cdot 10^6$ molec. $cm^{-3}\,s^{-1}$ in August. The winter values were generally below $2{\cdot}10^5$ $cm^{-3}\,s^{-1}$. Roughly two thirds of the turn-over rate were due to reactions with OH. Among all monoterpenes, α-pinene was the species with the highest mixing ratio and, in most months, highest turn-over rates. The turn-over rate of aromatics and monoterpenes can be used to roughly estimate the production rate of semivolatile organic compounds. Products from photooxidation of α- and β-pinene, such as pinonic acid, pinic, and norpinonic acid, have been identified in the aerosol phase in a number of chamber studies (Hoffmann et al., 1997) and recently in forest air (Kavouras et al., 1999). Our results from HAFEX suggest that the contribution of anthropogenic aromatics to aerosol formation is negligible compared to that of biogenic in the rural background air. Another essential, and surprising result was that the seasonal distribution of NPF events at Hohenpeissenberg (Fig. 6) is inverse to the seasonal cycle of terpene turn-over rates (Fig. 16b). Furthermore, we found no evidence for significantly enhanced monoterpene turn-over rates on days with NPF events, indicating that the corresponding contribution from potential biogenic aerosol precursors was either not detectable and/or negligible, or that other factors are more important in controlling a NPF event to develop or not.

However, the HAFEX results confirm a clear seasonal link between the production rates of biogenic aerosol precursors and the growth rates of newly formed aerosol

ACPD
2, 1655–1697, 2002

© EGU 2002

particles. Both seasonal cycles show a coincident maximum in summer (compare the Figs. 14a–b and 16b). Using the summer maximum of the monoterpene turn-over rate (which are a measure for the production rate of semivolatile products from photo-oxidation of terpenes) and the corresponding reaction yields of condensable products between 1 and 10% (Hoffmann et al., 1997), we determined mid-day production rates of semivolatile products in a range $6{\cdot}10^4$–$6{\cdot}10^5$ molec.cm^{-3} s^{-1}. These figures are up to 1 magnitude higher than the calculated production rates of H_2SO_4 from atmospheric SO_2 oxidation by OH, which were $< 5 \cdot 10^4$ cm^{-3} s^{-1} on a monthly average. In conclusion, the potential growth rate of nucleation mode particles by condensation of semi-volatile organic species may easily exceed the growth rates based on $H_2SO_4/H_2O/NH_3$, and could possibly account for part of the missing growth rate determined in the previous section.

7. Conclusions

Atmospheric new particle formation (NPF) events were detected and classified over a period of 2.5 years of observations. NPF events occurred on 18% of all measurement days, typically during midday hours under relatively sunny and low humidity conditions. Most NPF events during HAFEX occurred in spring and winter, but no intensive events were observed in summer. This is a surprising overall result since the potential aerosol precursor concentrations (H_2SO_4, monoterpenes) showed a clear maximum in summer. The horizontal dimensions of the air masses in which NPF events occur was estimated to be on the order of $\sim$ 100 km, while concurrent measurements at two different altitudes suggested an almost homogeneous distribution of newly formed particles across at least the lowest 300 m of the boundary layer. The observed concentrations of newly formed particles correlated significantly with solar irradiance and ambient levels of H_2SO_4, whereas an anti-correlation was observed with relative humidity and the condensational sink related to the pre-existing particle surface area. This was more pronounced in the cold season, when particle formation events were frequently associated with the advection of warm and dry air from southerly directions.

ACPD
2, 1655–1697, 2002

© EGU 2002

The observed particle formation rates during NPF events were calculated to be on average 1.11 $cm^{-3} s^{-1}$, with the range: 0.013–8.8 $cm^{-3} s^{-1}$. The binary homogeneous H_2SO_4-H_2O nucleation rates calculated from measured H_2SO_4 were scattered across a wide range of 30 orders of magnitude, and proved to be lower by several orders of magnitude than the experimental estimates, even when assuming particle formation in the thermodynamically more favourable top of the boundary layer region. The growth rates of nucleation mode particles showed a seasonal cycle with higher growth rates up to 9 $nm\,h^{-1}$ in the summer and below 3 $nm\,h^{-1}$ in the months October to February. A fraction of the particle growth rates (occasionally close to 100%) was explained by the co-condensation of H_2SO_4/H_2O/NH_3. In most cases, however, this fraction account for 50% or less of the observed growth rates. This gap could potentially be filled by condensable organic vapours: based on calculated atmospheric turn-over rates it may be expected that the oxidation products of monoterpenes contribute significantly to the observed particle growth especially in the warm season. However, the calculated terpene turn-over rates did not show a significant correlation with the "missing" particle growth rate, which might be a consequence of the restricted data available and the simplistic assumption that turn-over is a measure for condensational growth due to organics. Another question emerged behind the duration of the observed linear nucleation mode particle growth, which often lasted well beyond the mid-day period when photochemically produced vapours were high. Although a large set of observational data is now available, the mechanisms that ultimately control the development of NPF events are not understood. The role of sulfuric acid and of low condensational sink due to pre-existing particles was demonstrated on a statistical basis, however, individual cases of NPF events were observed at low H_2SO_4 concentrations and/or high condensational sinks. Furthermore, no indications were found that the availability of reaction products of organic compounds would control the occurrence of NPF events. Another yet unresolved question refers to the closed particle size distributions during NPF events, showing lower concentrations at the lower end (3–5 nm) than at 5–10 nm: This cannot be explained assuming an in-situ production and subsequent linear growth

ACPD
2, 1655–1697, 2002

© EGU 2002

of nano-particles. Either measurements in this size range are prone to systematic errors (which appears, however, unlikely in view of the instrumental characterisations and tests carried out), or other mechanisms than the condensation of photochemically produced vapours are important. The identification of the mechanisms that ultimately control the development of NPF events will require a more detailed modelling of the nano-particle size distribution evolution, which need to be addressed in future studies.

Acknowledgements. We highly appreciate the support by Dr W. Fricke and Dr P. Winkler, and especially thank U. Kaminski for providing CPC data. R. Wilhelm, P. Settele, R. Ruf, K. Michl and G. Stange (all at MOHp) are highly acknowledged for their technical assistance. We also thank Dr D. Covert for his valuable comments to the manuscript. This work was performed under BMBF grants 07AF201A/8 and B/8.

References

Berresheim, H., Elste, T., Plass-Dülmer, C., Eisele, F. L., and Tanner, D. J.: Chemical ionization mass spectrometer for long-term measurements of atmospheric OH and H_2SO_4, Int. J. Mass Spectrom., 210-211, 2000. 1659

Birmili, W. and Wiedensohler, A.: New particle formation in the continental boundary layer: Meteorological and gas phase parameter influence, Geophys. Res. Lett., 27, 3325–3328, 2000. 1657, 1664

Birmili, W., Stratmann, F., Wiedensohler, A., Covert, D., Russell, L. M., and Berg, O.: Determination of differential mobility analyzer transfer functions using identical instruments in series, Aerosol Sci. Technol., 27, 215–223, 1997. 1663

Birmili, W., Stratmann, F., and Wiedensohler, A.: Design of a DMA-based size spectrometer for a large particle size range and stable operation, J. Aerosol Sci., 30, 549–553, 1999. 1659

Birmili, W., Wiedensohler, A., Plass-Dülmer, C., and Berresheim, H.: Evolution of newly formed aerosol particles in the continental boundary layer: A case study including OH and H_2SO_4 measurements, Geophys. Res. Letters, 27, 2205–2209, 2000. 1661, 1672

Clarke, T. D.: Atmospheric nuclei in the Pacific midtroposphere: Their nature, concentration and evolution, J. Geophys. Res., 98D, 20 633–20 647, 1993. 1657

Clement, C. F., Pirjola, L., dal Maso, M., Mäkelä, J. M., and Kulmala, M.: Analysis of particle formation bursts observed in Finland, J. Aerosol Sci., 32, 217–236, 2001. 1667

© EGU 2002

Coe, H., Williams, P., McFiggans, G., Gallagher, M., Beswick, K., Bower, K., and Choularton, T.: Behavior of ultrafine particles in continental and marine air masses at a rural site in the united kingdom, J. Geophys. Res., 105, 26 891–26 905, 2000. 1662
Coffman, D. J. and Hegg, D. A.: A preliminary study of the effect of ammonia on particle nucleation in the marine boundary layer, J. Geophys. Res., 100, 7147–7160, 1995. 1657
Covert, D. S., Kapustin, V. N., Quinn, P. K., and Bates, T. S.: New particle formation in the marine boundary layer, J. Geophys. Res., 97, 20 581–20 589, 1992. 1657
Easter, R. C. and Peters, L. K.: Binary homogeneous nucleation: Temperature and relative humidity fluctuations, nonlinearity, and aspects of new particle formaton in the atmosphere, J. Appl. Met., 33, 775–784, 1994. 1657
Friedlander, S. K.: Smoke, Dust, and Haze, Oxford University Press, New York, 2000. 1671
Guenther, A. B., Zimmerman, P. R., Harley, P. C., Monson, R. K., and Fall, R.: Isoprene and monoterpene emission rate variability: model evaluations and sensitivity analyses, J. Geophys. Res., 98, 12 609–12 617, 1993. 1673
Haywood, J. and Boucher, O.: Estimates of the direct and indirect radiative forcing due to tropospheric aerosols: A review, Rev. Geophys., 38, 513–543, 2000. 1656
Hoffmann, T., Odum, J. R., Bowman, F., Collins, D., Klockow, D., Flagan, R. C., and Seinfeld, J. H.: Formation of organic aerosols from the oxidation of biogenic hydrocarbons, J. Atmos. Chem., 26, 189–222, 1997. 1673, 1674
Holzworth, C. G.: Estimates of mean maximum mixing depths in the contiguous United States, Mon. Wea. Rev., 92, 235–242, 1964. 1669
Hõrrak, U., Salm, J., and Tammet, H., Bursts of intermediate ions in atmospheric air, J. Geophys. Res., 103, 13 909–13 915, 1998. 1657
Hõrrak, U., Salm, J., and Tammet, H.: Statistical characterisation of air ion mobility spectra at tahkuse observatory: Classification of air ions, J. Geophys. Res., 105, 9291–9302, 2000. 1664
Houghton, J., Ding, Y., Griggs, D., Noguer, M., van der Linden, P., and Xiaosu, D.: (Eds) Climate Change 2001: The Scientific Basis, IPCC, Cambridge Univ. Press, contribution of Working Group I to the Third Assessment Report of the Intergovernmental Panel on Climate Change (IPCC), 2001. 1657
Karg, E., Ferron, G. A., Busch, B., and Heyder, J.: Growth behaviour and aqueous fraction of atmoshperic particles in dependence of relative humidity (translated from German), Final report BII7 BayFORKLIM, GSF, Neuherberg, Germany, 1999. 1659

© EGU 2002

Kavouras, I., Mihalopoulos, N., and Stephanou, E. G.: Secondary aerosol formation vs. primary organic aerosol emission: In situ evidence for the chemical coupling between monoterpene acidic photo-oxidation products and new particle formation over forests, Env. Sci. Technol., 33, 1028–1037, 1999. 1673

Kerminen, V.-M., Pirjola, L., and Kulmala, M.: How significantly does coagulational scavenging limit atmospheric particle production?, J. Geophys. Res., 125, 24 110–24 125, 2001. 1661

Korhonen, P., Kulmala, M., Laaksonen, A., Viisanen, Y., McGraw, R., and Seinfeld, J. H.: Ternary nucleation of H_2SO_4, NH_3, and H_2O in the atmosphere, J. Geophys. Res., 104, 26 349–26 354, 1999. 1668, 1670

Kulmala, M., Hämeri, K., Aalto, P., et al.: Overview of the international project on biogenic aerosol formation in the boreal forest (BIOFOR), Tellus, 53B, 324–343, 2001. 1657, 1662

Kulmala, M., Laaksonen, A., and Pirjola, L.: Parametrizations for sulphuric acid/water nucleation rates, J. Geophys. Res., 103, 8301–8307, 1998. 1669

Kulmala, M., Pirjola, L., and Mäkelä, J. M.: Stable sulphate clusters as a source of new atmospheric particles, Nature, 404, 66–69, 2000. 1657, 1670

Mäkelä, J. M., Aalto, P., Jokinen, V., Pohja, T., Nissinen, A., Palmroth, S., Markkanen, T., Seitsonen, K., Lihavainen, H., and Kulmala, M.: Observation of ultrafine aerosol particle formation and growth in boreal forest, Geophys. Res. Letters, 24, 1219–1222, 1997. 1657

Mäkelä, J. M., Dal Maso, M., Pirjola, L., Keronen, P., Laakso, L., Kulmala, M., and Laaksonen, A.: Characteristics of the aerosol particle formation events observed at a boreal forest site in southern Finland, Boreal Env. Res., 5, 299–313, 2000. 1664

O'Dowd, C., Jimenez, J., Bahreini, R., Flagan, R., Seinfeld, J., Hämeri, K., Pirjola, L., Kulmala, M., Jennigns, S., and Hoffmann, T., Marine aerosol formation from biogenic iodine emissions, Nature, 417, 632–636, 2002a. 1657

O'Dowd, C. D., Hämeri, K., Aalto, P., and Kulmala, M., First experimental evidence of new particle formation from organic vapours over forests, Nature, 416, 497–498, 2002b. 1657

McMurry, P. H., Woo, K. S., Weber, R., Chen, D.-R., and Pui, D. Y. H.: Size distributions of 3 to 10 nm atmospheric particles: Implications for nucleation mechanisms, Phil. Trans. Royal Soc., A358, 2625–2642, 2000. 1662

Nilsson, E. D. and Kulmala, M.: The potential for atmospheric mixing processes to enhance the binary nucleation rate, J. Geophys. Res., 103, 1381–1389, 1998. 1657

Raes, F.: Entrainment of free tropospheric aerosols as a regulating mechanism for cloud condensation nuclei in the remote boundary layer, J. Geophys. Res., 100, 2893–2903, 1995.

© EGU 2002

1657
Ravishankara, A. R.: Heterogeneous and multiphase chemistry in the troposphere, Science, 276, 1058–1065, 1997. 1656
Reischl, G. P., Mäkelä, J. M., and Necid, J.: Performance of a Vienna type differential mobility analyzer at 1.2–20 nanometer, Aerosol Sci. Technol., 27, 651–672, 1997. 1663
Seinfeld, J. H. and Pandis, S. P.: Atmospheric Chemistry and Physics, John Wiley, New York, 2 edn., 1998. 1666
Spindler, G., Teichmann, U., and Sutton, M. A.: Ammonia dry deposition over grassland-micrometeorological flux-gradient measurements and bidirectional flux calculations using an inferential model, Q. J. Royal Met. Soc., 127, 795–814, 2001. 1670
Swietlicki, E., Zhou, J., Berg, O. H., Martinsson, M. G., Frank, G., Cederfelt, S. I., Dusek, U., Berner, A., Birmili, W., Wiedensohler, A., Yuskiewicz, B., and Bower, K. N.: A closure study of sub-micrometer aerosol particle hygroscopic behaviour, Atmos. Res., 50, 205–240, 1999. 1659
Weber, R. J., Marti, J. J., McMurry, P. H., Eisele, F. L., Tanner, D. J., and Jefferson, A.: Measurement of new particle formation and ultrafine particle growth rates at a clean continental site, J. Geophys. Res., 102, 4375–4385, 1997. 1657
Weber, R. J., McMurry, P. H., III, R. L. M., Tanner, D. J., Eisele, F. L., Clarke, A. D., and Kapustin, V. N.: New particle formation in the remote troposphere: A comparison of observations at various sites, Geophys. Res. Lett., 26, 307–310, 1999. 1657
Wiedensohler, A.: An approximation of the bipolar charge distribution for particles in the submicron range, J. Aerosol Sci., 19, 387–389, 1988. 1663
Wiedensohler, A., Covert, D. S., Swietlicki, E., Aalto, P., Heintzenberg, J., and Leck, C.: Occurrence of an ultrafine particle mode less than 20 nm in diameter in the marine boundary layer during Arctic summer and autumn, Tellus, 48B, 213–222, 1996. 1657
Winklmayr, W., Reischl, G. P., Linde, A. O., and Berner, A.: A new electromobility spectrometer for the measurement of aerosol size distributions in the size range from 1 to 1000 nm, J. Aerosol Sci., 22, 289–296, 1991. 1659
WMO2001, Global Atmosphere Watch, World Meteorological Organization: http://www.wmo.ch/web/arep/gaw_home.html, 2001. 1658
Yu, F. and Turco, R. P.: Ultrafine aerosol formation via ion-mediated nucleation, Geophys. Res. Letters, 27, 883–886, 2000. 1657

© EGU 2002

Table 1. Criteria for NPF event definition, based on parameters derived from the diurnal cycles of $N_{[3;11]}$ and N_{tot}

	Parameter Name	Range	Parameter is indicator of
(a)	plateau concentration of $N_{[3;11]}$	$> 1000\,cm^{-3}$	particle formation intensity
(b)	time for $N_{[3;11]}$ to increase	< 4 hours	significant diurnal cycle in $N_{[3;11]}$
(c)	time for $N_{[3;11]}$ to decline	< 7 hours	significant diurnal cycle in $N_{[3;11]}$
(d)	fraction of UFPs ($N_{[3;11]}/N_{tot}$)	> 0.15	significant particle formation

ACPD
2, 1655–1697, 2002

© EGU 2002

Table 2. Mean daily fit maximum values of the parameters global radiation, solar irradiance (seasonally normalised), and H_2SO_4 for different event classes. p_0 indicates the maximum error probability at which the hypothesis H_0: $\mu_{x,i} > \mu_{x,0}$ is accepted (one-sided two-sample Gauss test)

	H_2SO_4, cm^{-3}			solar irradiance, $W\,m^{-2}$			Global Rad. (normalised)		
	μ_x	$\sigma(\mu_x)$	p_0	μ_x	$\sigma(\mu_x)$	p_0	μ_x	$\sigma(\mu_x)$	p_0
Non-Events	4.10	0.28		504	13		0.69	0.013	
Event, I	10.29	1.57	0.9999	682	56	0.9988	0.89	0.034	0.9999
Event, II	7.46	1.08	0.9985	602	31	0.9983	0.89	0.020	0.9999
Event, III	5.57	1.15	0.8893	528	37	0.7234	0.78	0.036	0.9908

ACPD
2, 1655–1697, 2002

© EGU 2002

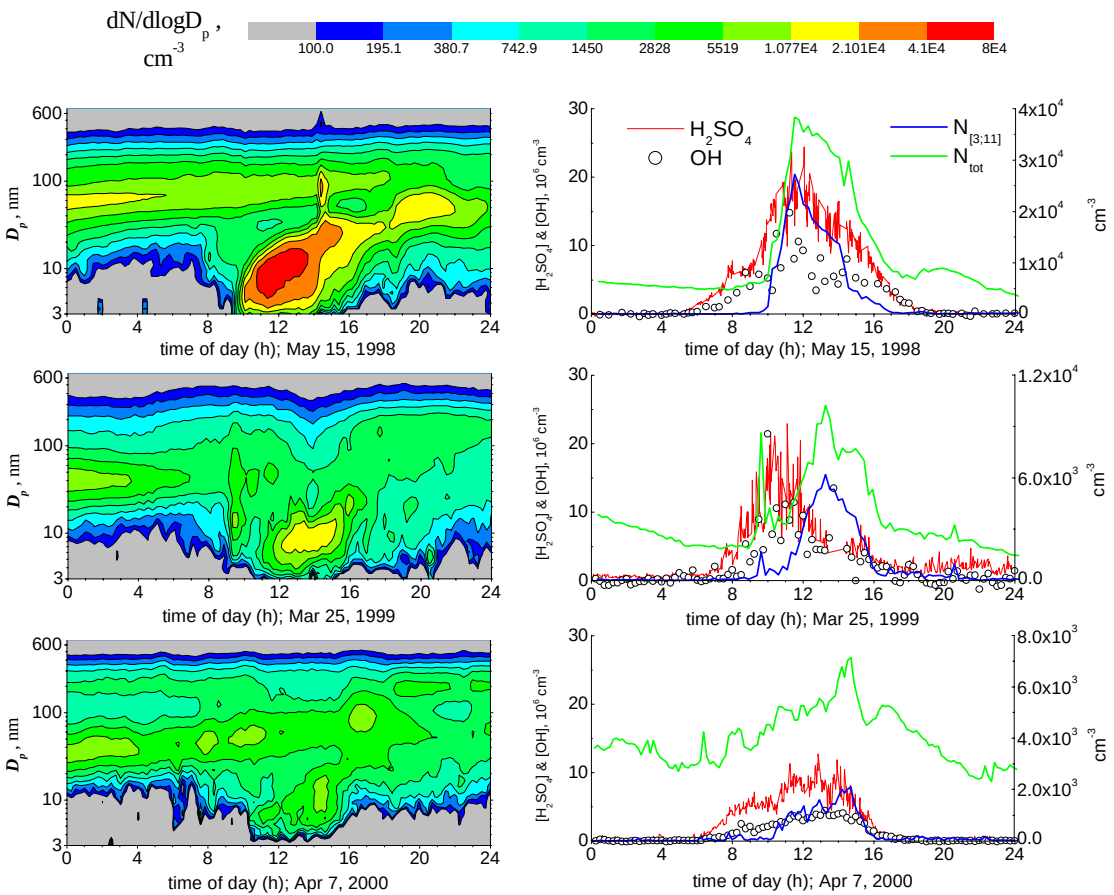

Fig. 1. Three days illustrating different intensities of new particle formation events at Hohenpeissenberg. Diurnal evolution of the particle number size distribution (left), UFP ($N_{[3;11]}$, total particle number (N_{tot}), H_2SO_4, and OH concentrations (right).

ACPD
2, 1655–1697, 2002

The Hohenpeissenberg aerosol formation experiment (HAFEX)

Birmili et al.

© EGU 2002

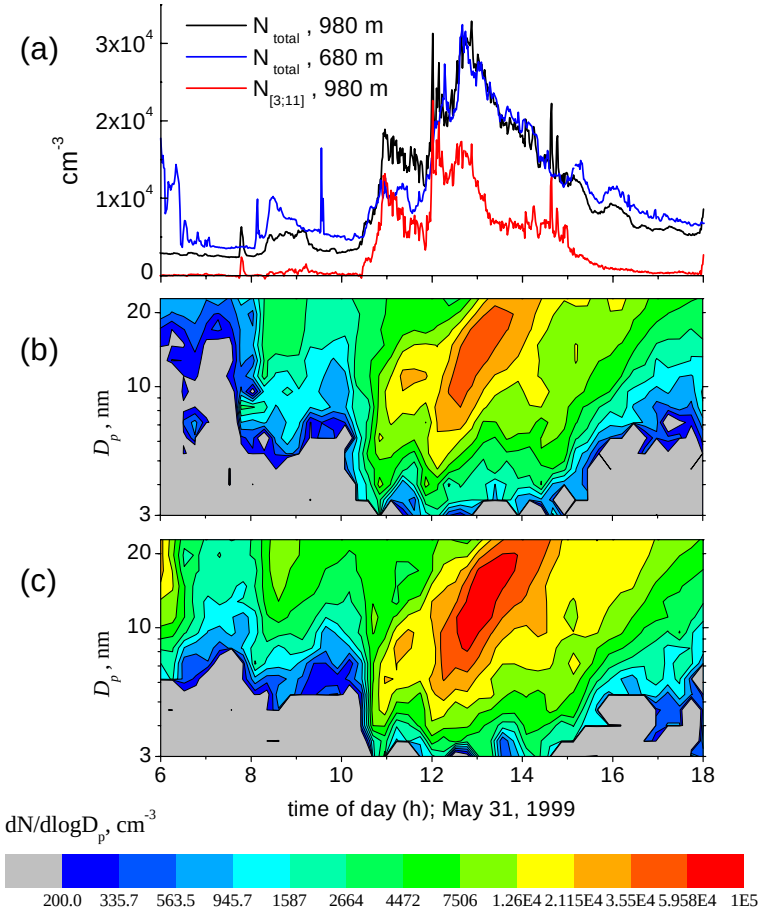

Fig. 2. A new particle formation event (31 May 1999) observed simultaneously at two different levels of altitude: **(a)** Total particle and UFP concentrations at MOHP (980 m) and the low-level station (680 m), and evolution of the particle size distribution **(b)** at MOHP, and **(c)** at the low-level station.

ACPD
2, 1655–1697, 2002

The Hohenpeissenberg aerosol formation experiment (HAFEX)

Birmili et al.

© EGU 2002

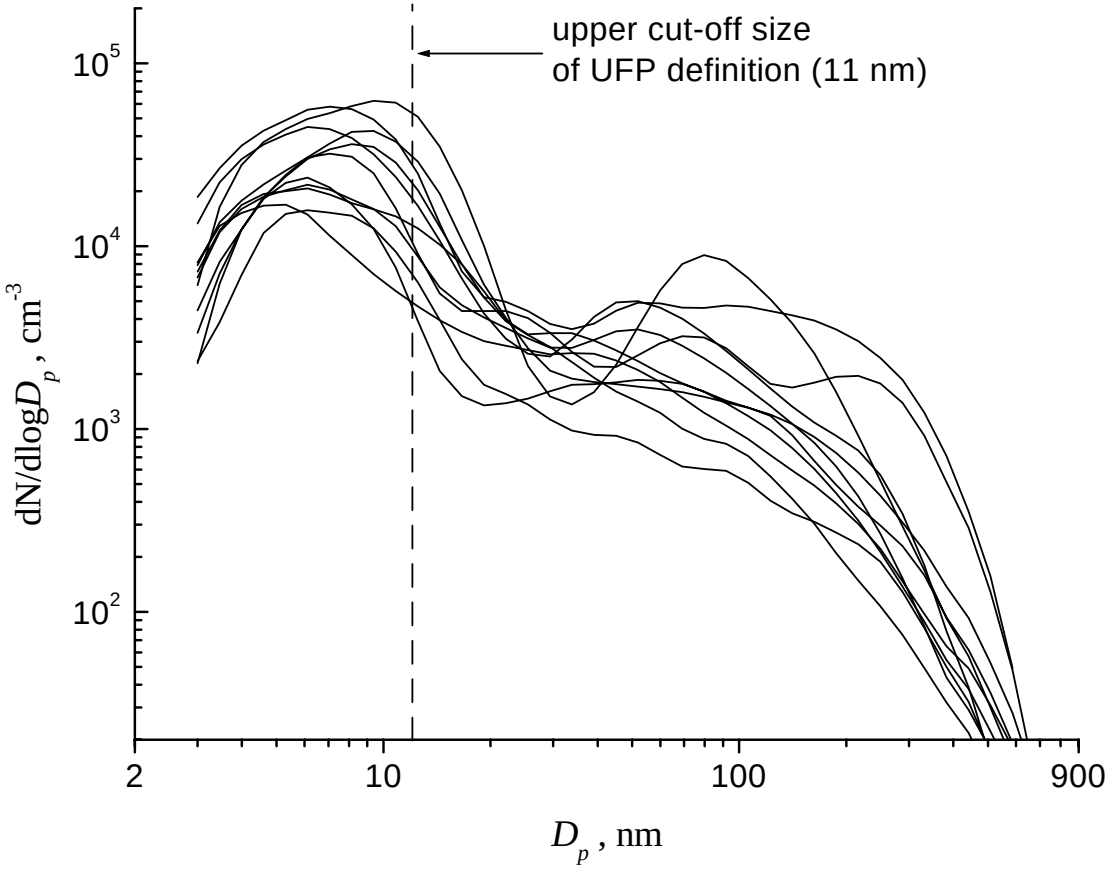

Fig. 3. Particle size distributions measured during NPF events with high UFP fraction (> 0.58). The events shown date from 980401, 980407, 980420, 980515, 980519, 981226, 981228, 981108, 990103, 990106, and 990314.

ACPD

2, 1655–1697, 2002

The Hohenpeissenberg aerosol formation experiment (HAFEX)

Birmili et al.

© EGU 2002

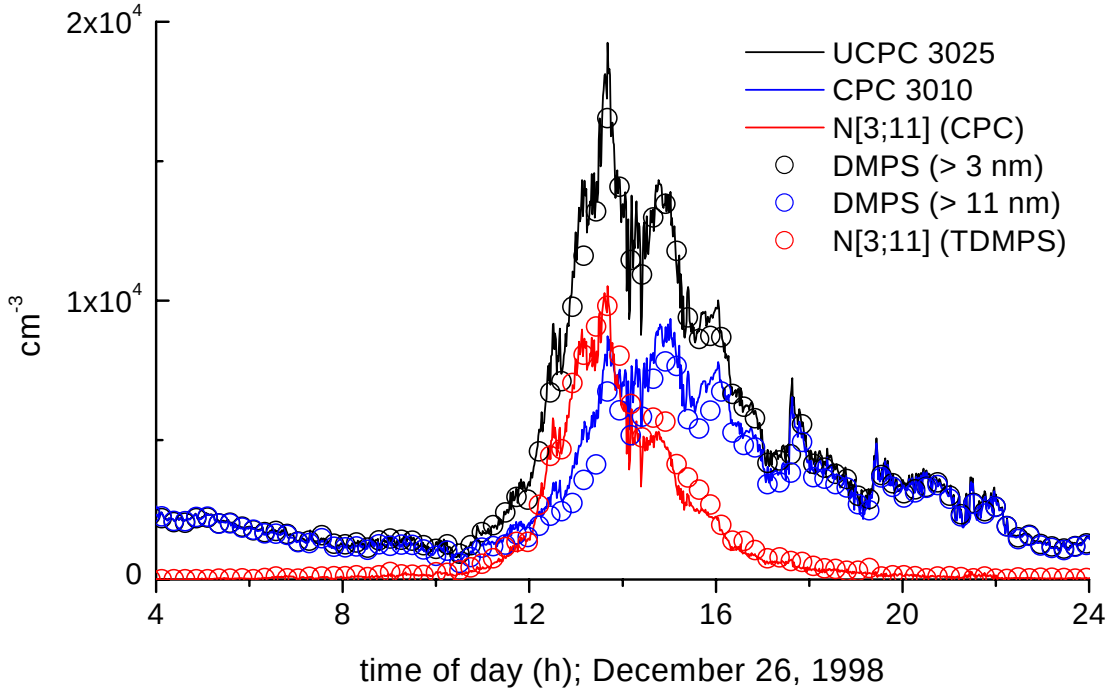

Fig. 4. Comparison between total and UFP number concentration derived from two CPCs with different lower detection limit, and the TDMPS, respectively. More data of this event is shown in Fig. 13.

ACPD
2, 1655–1697, 2002

© EGU 2002

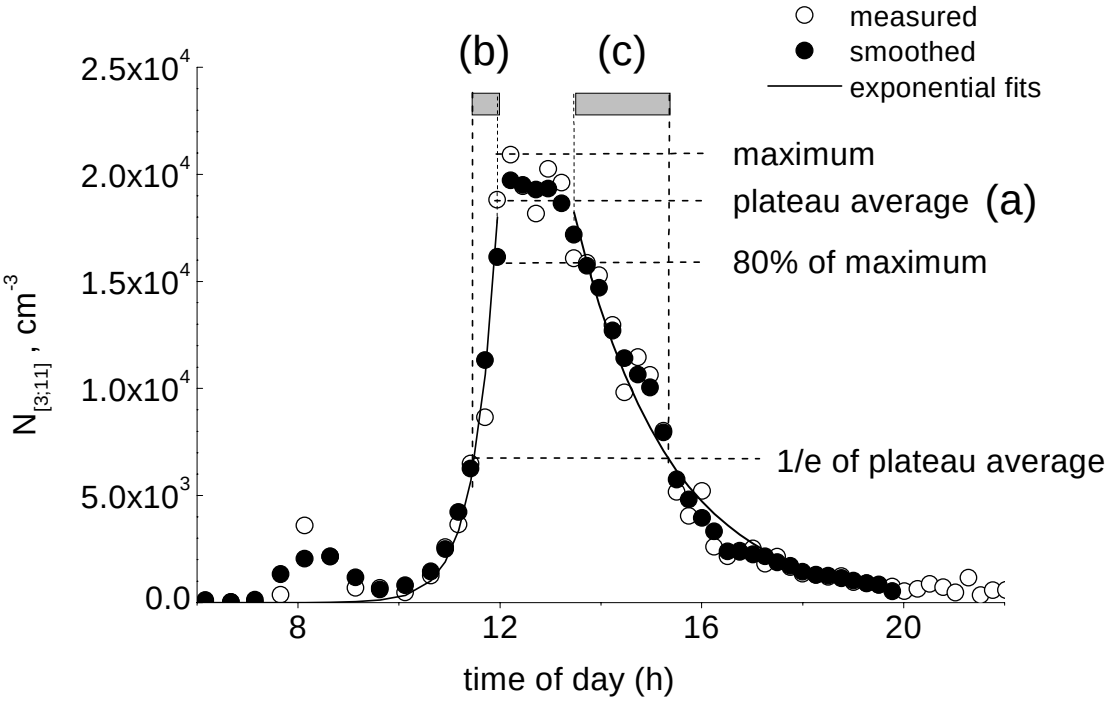

Fig. 5. Detection of new particle formation events based on the diurnal cycle of $N_{[3;11]}$. Data is from 20 April 1998. For explanation of the parameters **(a)**, **(b)**, and **(c)**, see Sect. 4.1.

ACPD
2, 1655–1697, 2002

© EGU 2002

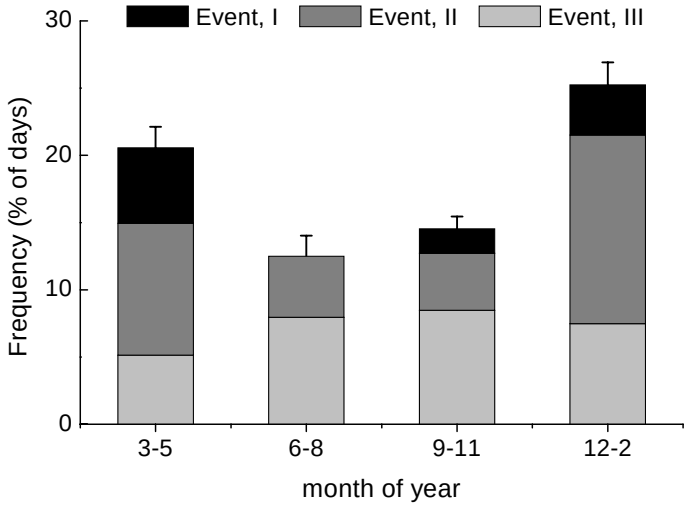

Fig. 6. Seasonal frequency of different classes of NPF events at Hohenpeissenberg (April 1998–August 2000).

ACPD
2, 1655–1697, 2002

© EGU 2002

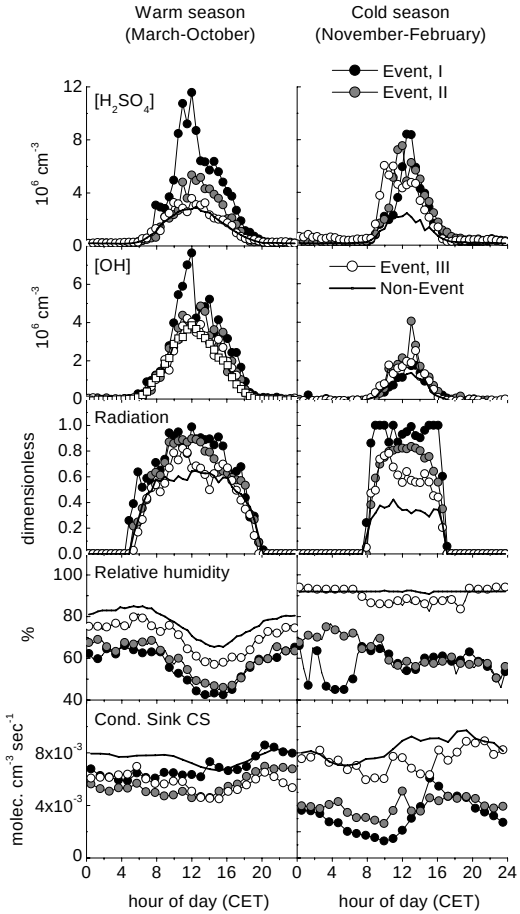

Fig. 7. Median diurnal cycles of [H_2SO_4], [OH], solar irradiance, relative humidity (RH), and the condensational sink CS (mean values), separated after different particle formation intensities. The diurnal cycles of solar irradiance were normalised by a cloudless radiation profile of the respective month (see text for more details). RHs > 94% were indistinguishable owing to limitations of the RH sensor.

ACPD
2, 1655–1697, 2002

The Hohenpeissenberg aerosol formation experiment (HAFEX)

Birmili et al.

© EGU 2002

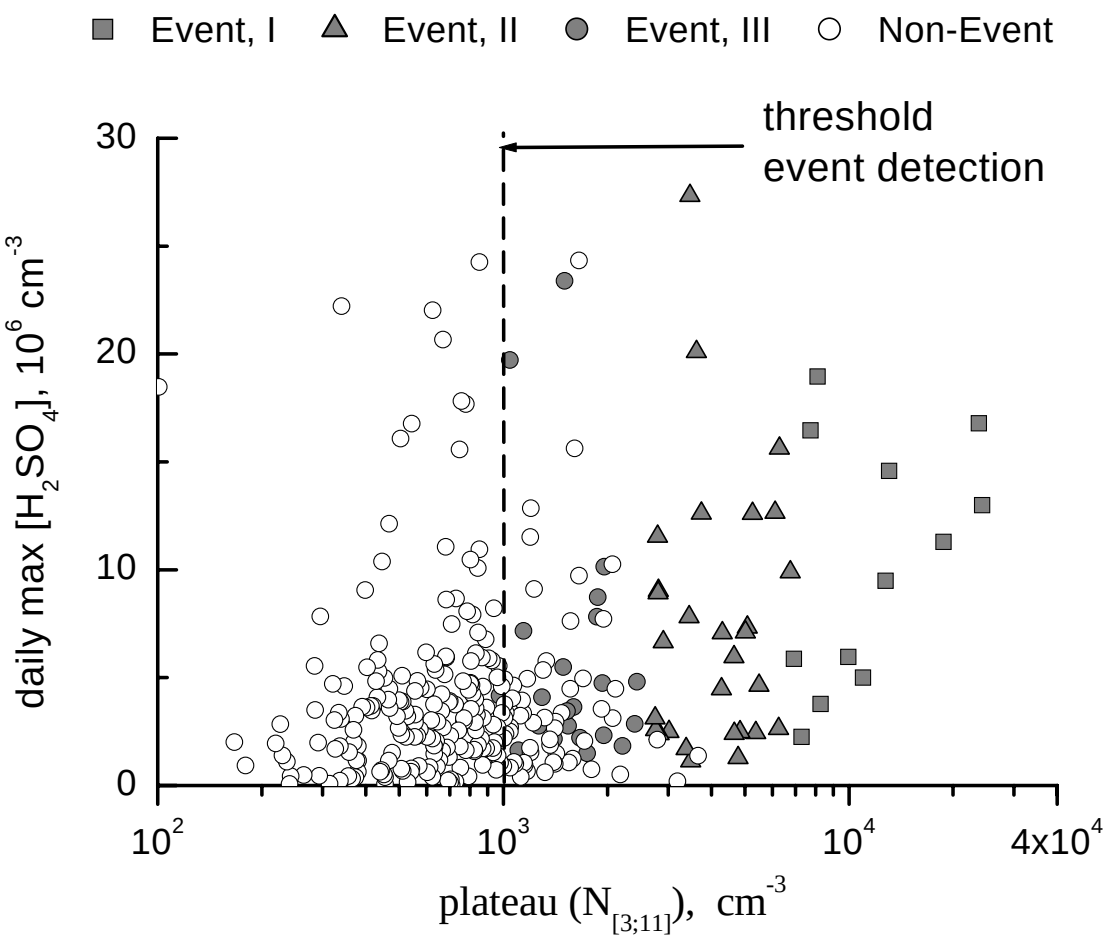

Fig. 8. Cross-correlation between the observed UFP plateau (≈maximum) concentration and the daily peak concentration of H_2SO_4 for the entire set of event and non-event days.

ACPD

2, 1655–1697, 2002

The Hohenpeissenberg aerosol formation experiment (HAFEX)

Birmili et al.

© EGU 2002

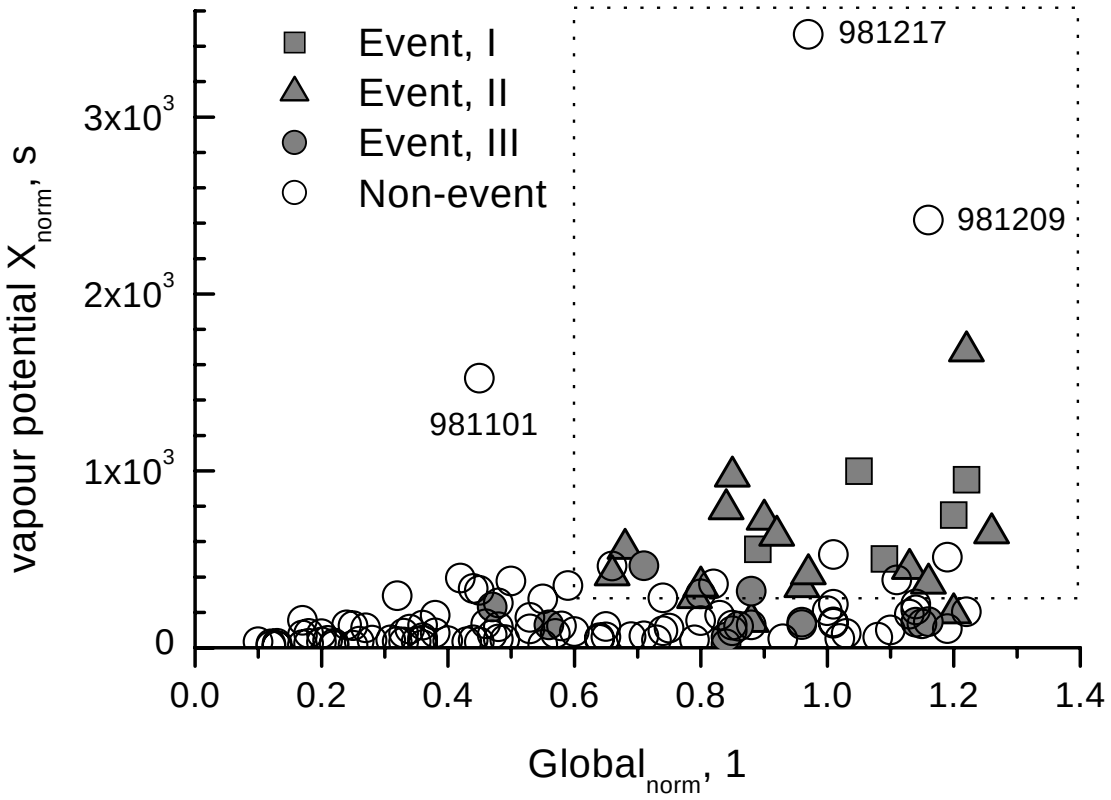

Fig. 9. Daily peak concentrations of vapour availability X_{norm} vs. normalised solar irradiance (data from the cold season only). The dashed rectangle describes a parameter space that encompasses 90% of all class I-II events, while only allowing for 6% of the non-events.

ACPD
2, 1655–1697, 2002

© EGU 2002

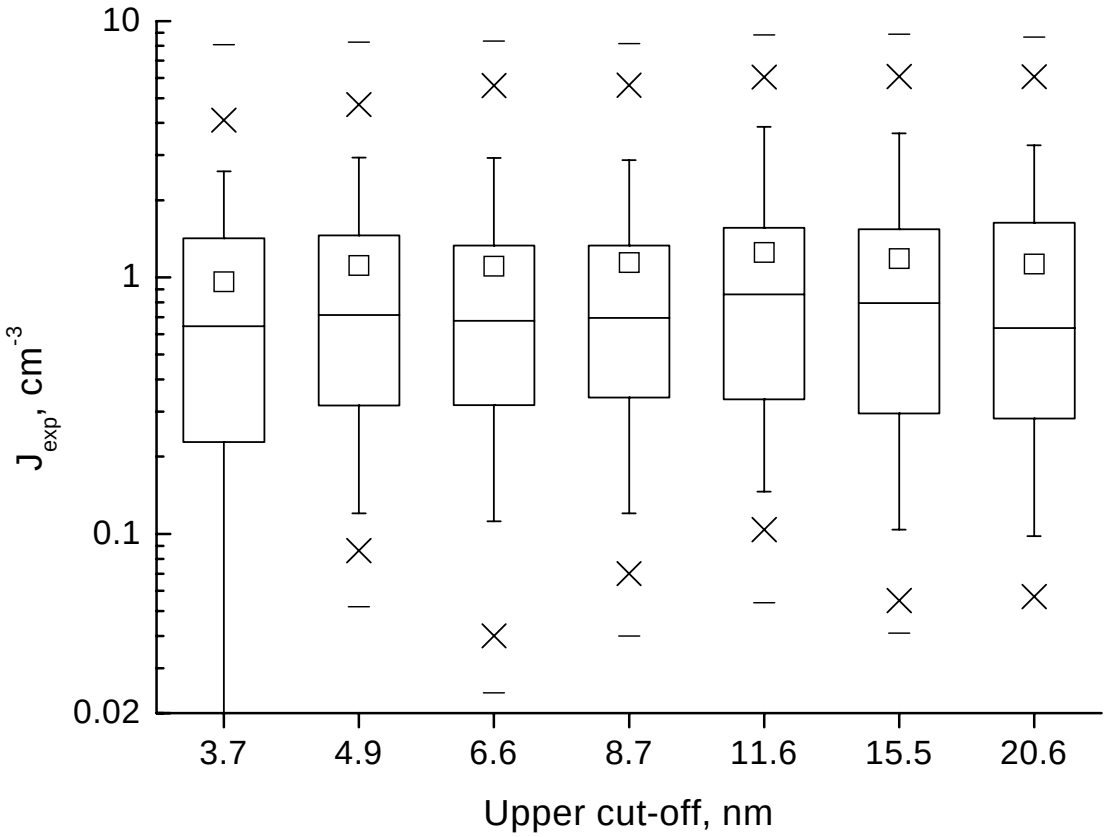

Fig. 10. The experimental particle formation rates as a function of the upper size cut-off defining the range of UFPs. Box-and-whisker plot indicate median and quartiles (box), mean (squares), 90% quantile (whiskers), 95% quantile (crosses) and maximum values (bars).

ACPD
2, 1655–1697, 2002

© EGU 2002

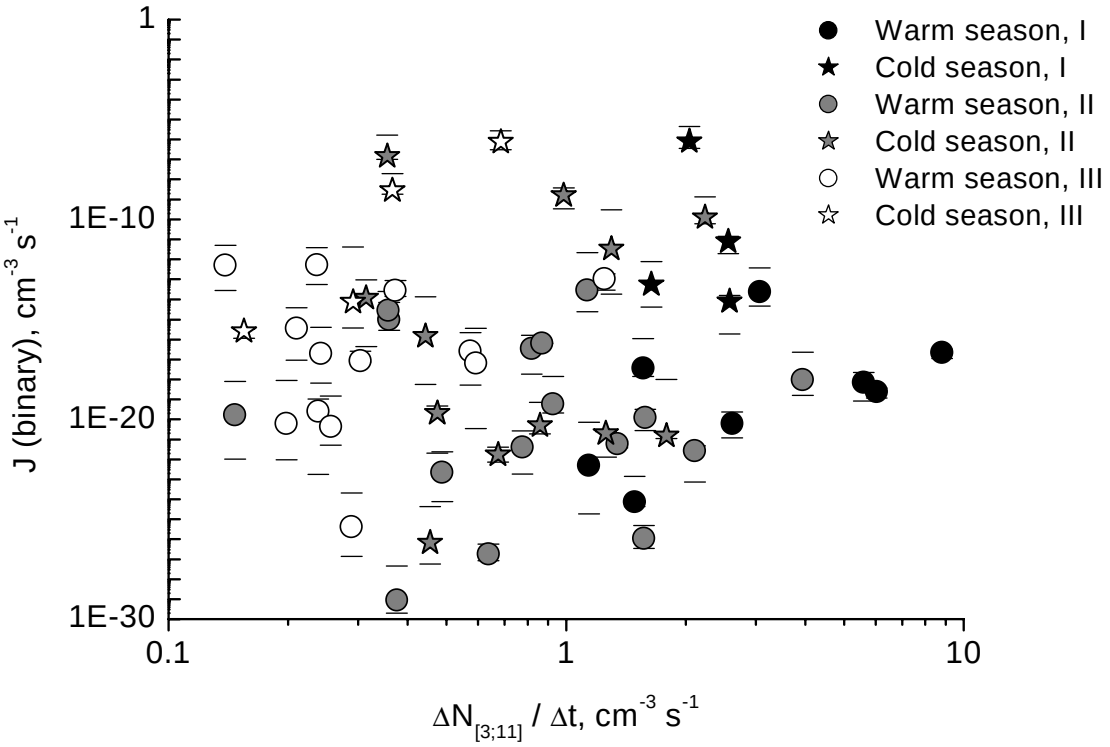

Fig. 11. Comparison between an "apparent" particle formation rate $\Delta N_{[3;11]}/\Delta t$ with the binary nucleation rate (H_2SO_4/H_2O) for measured H_2SO_4.

ACPD
2, 1655–1697, 2002

© EGU 2002

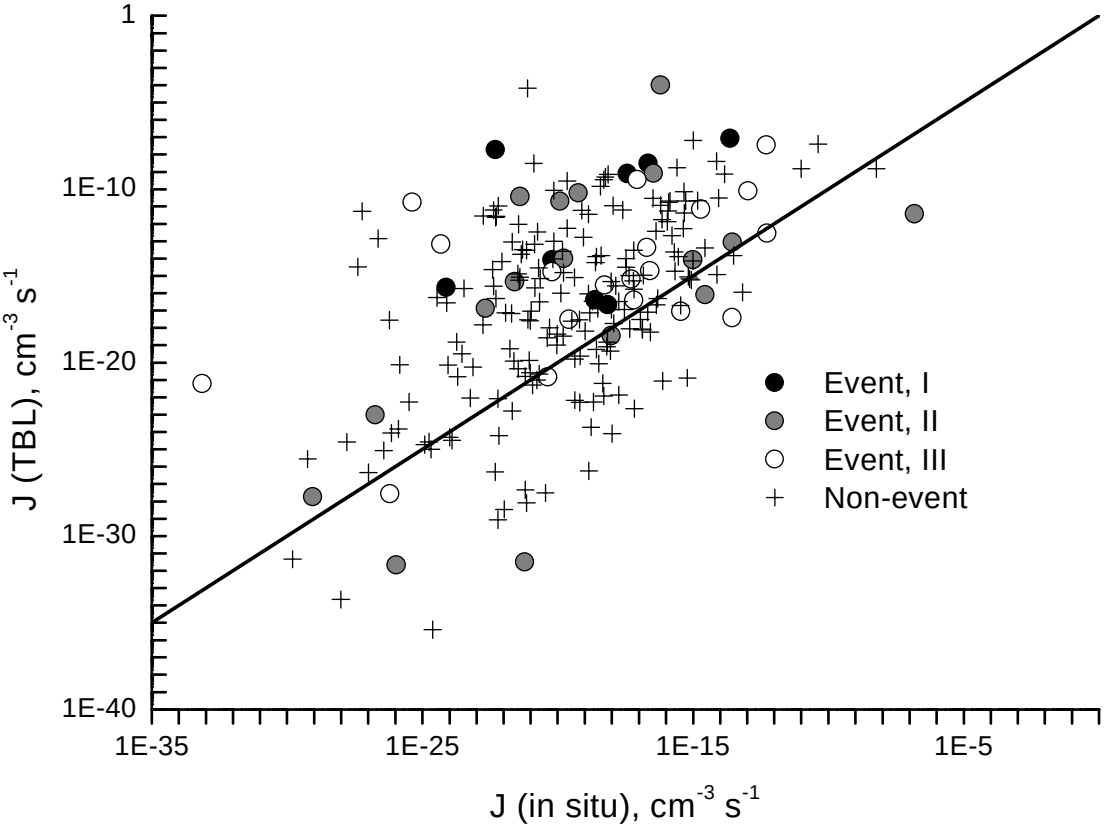

Fig. 12. Calculated binary H_2SO_4/H_2O nucleation rates: Comparison between in-situ rates at the observation point (abscissa) and rates on top of the boundary layer (TBL). The rates were calculated assuming a homogeneously distributed H_2SO_4 across the boundary layer depth. The solid line is the unity curve. Star symbols indicate the calculated rates for non-event days, for comparison.

ACPD
2, 1655–1697, 2002

© EGU 2002

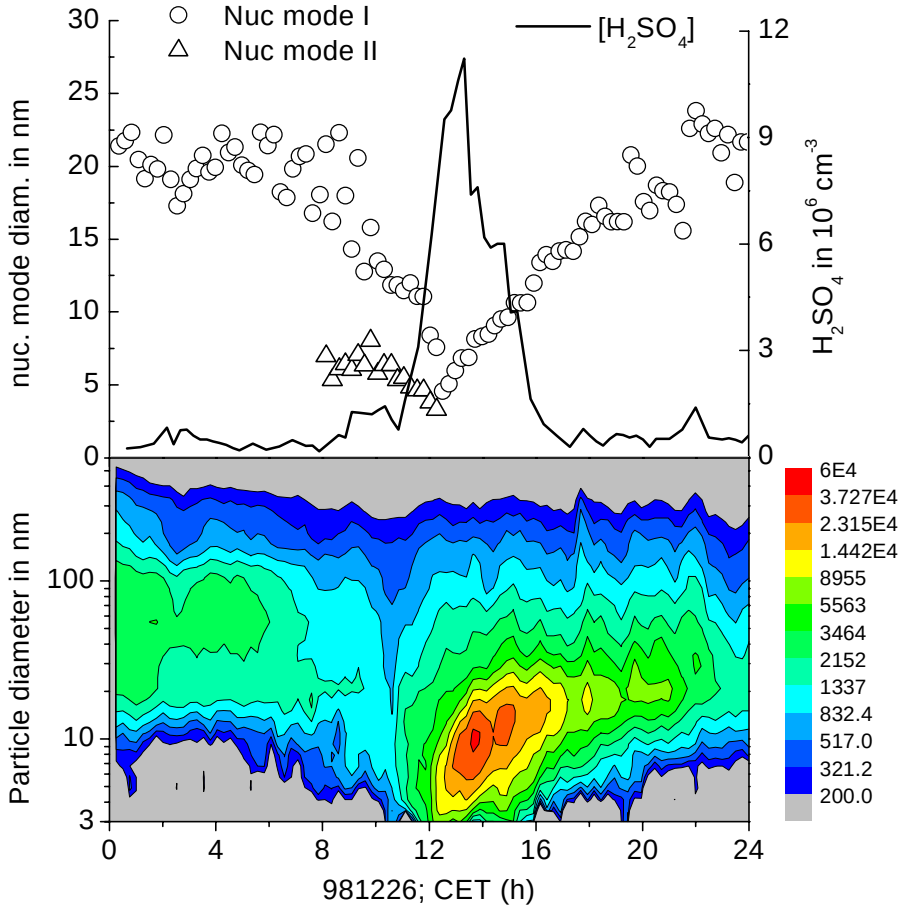

Fig. 13. Time series of the particle size distribution ($dN/d\log D_p$ in cm^{-3}), the nucleation mode diameter, and H_2SO_4. Data is from 26 December 1998, a winter class I event day.

ACPD
2, 1655–1697, 2002

The Hohenpeissenberg aerosol formation experiment (HAFEX)

Birmili et al.

© EGU 2002

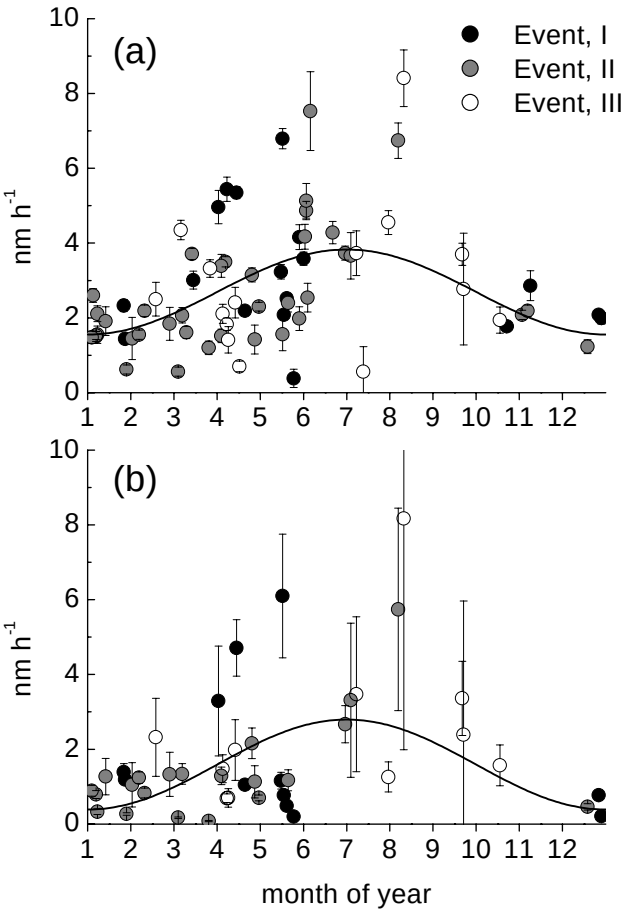

Fig. 14. Annual distribution of **(a)**, the experimentally determined growth rate of nucleation mode particles and **(b)**, the excess particle growth rate after subtraction of the term caused by $H_2SO_4/H_2O/NH_3$ condensation. Both graphs include a fit curve of the first harmonic.

ACPD
2, 1655–1697, 2002

© EGU 2002

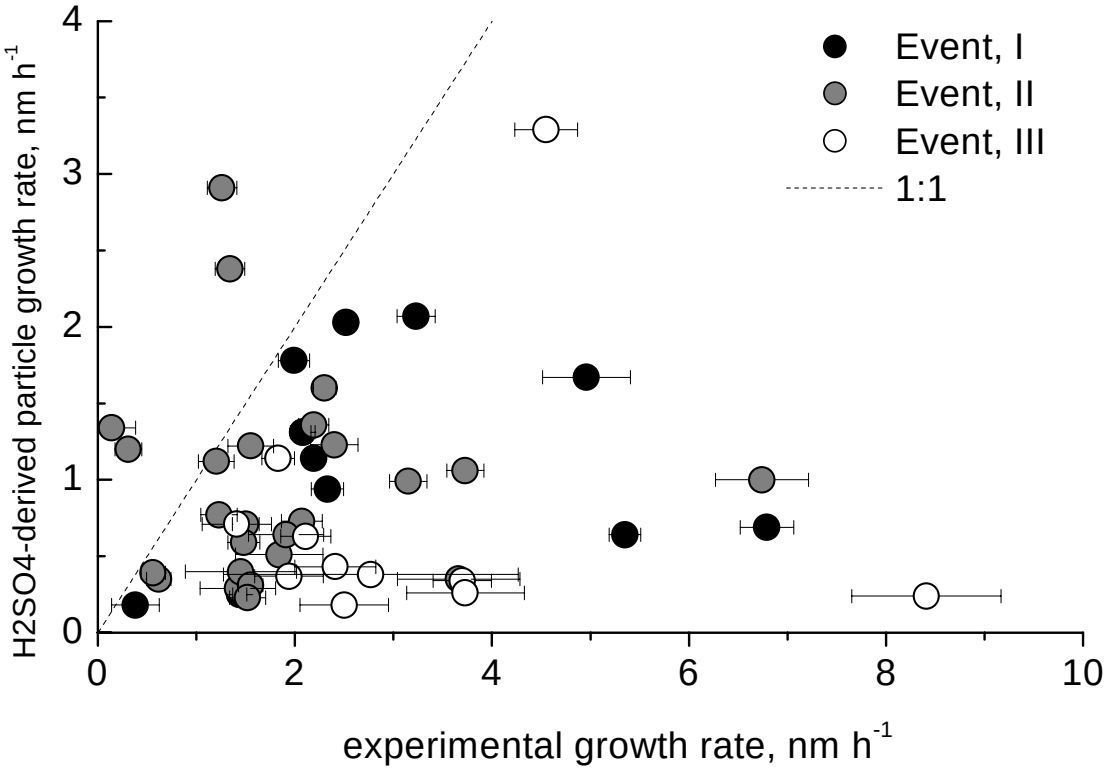

Fig. 15. Direct comparison between the experimentally and theoretically determined growth rate of nucleation mode particles.

ACPD
2, 1655–1697, 2002

© EGU 2002

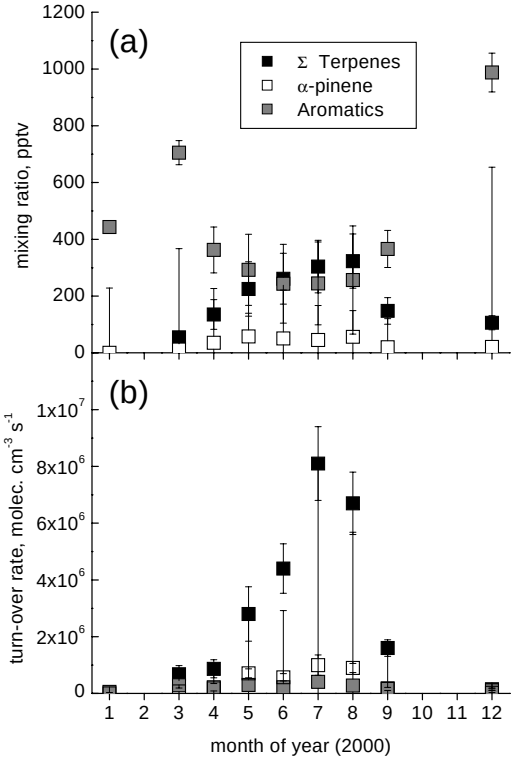

Fig. 16. **(a)** Monthly averages of the noontime (11:00–15:00 h) mixing ratios of the sum of C_6-C_9 aromatic hydrocarbons (circles), α-pinene (triangles), and the sum of all measured terpenes (diamonds) including α-pinene, β-pinene, Δ^3-carene, eucalyptol, limonene, camphene, myrcene, sabinene, tricyclene (in order of abundance), and traces of α-terpinene, γ-terpinene and terpinolene; **(b)** the corresponding noon time turnover rates due to reactions with OH and ozone. In case of OH the measured concentrations were used, in September and December for lack of concurrent OH measurements monthly noontime averages were used. The bars represent one sigma standard deviations.

ACPD
2, 1655–1697, 2002

© EGU 2002